

Low-Light Image Enhancement via Mixture L2-LP Variational Retinex Model with Adaptive Texture Map

Thesis Supervisor
Prof. Youji Iiguni

Kazuki Kurihara

Division of Systems Science and Applied Informatics
Department of Systems Innovation
Graduate School of Engineering Science
Osaka University

January 28, 2020

Contents

1	Introduction	1
2	Related Work	3
2.1	Retinex Theory	3
2.2	Variational Retinex Model	4
2.3	Local Variation Deviation	4
2.4	Consideration of Problems	6
3	Proposed Method	9
3.1	L2-LP Variational Model	9
3.2	Adaptive Texture Map	12
3.3	Solution	13
3.4	Effectiveness of the proposed method	15
4	Experiment	17

Chapter 1

Introduction

Images captured under low light conditions suffer from poor visibility, low contrast, and unexpected noise. It is difficult for human to extract hidden meaningful information from these images. Moreover, these degradation affect vision techniques, such as consumer digital camera, mobile phones and video surveillance system, which can be often used in outdoors. Therefore, many image enhancement methods, including histogram equalization (HE) algorithms [1] - [3], dehaze-based algorithms [4], [5], and Retinex-based algorithms[6] - [12] have been proposed to improve above problems.

HE algorithms are probably the most intuitive and simplest way to improve image contrast. The operation stretches the dynamic range of intensity level of an observed image. However, these methods may result in over-enhancement. In addition, these methods cannot consider the intensive noise hidden under dark regions in low light images. Thus, these methods lead to noise amplification after contrast enhancement.

Some researches [4], [5] noticed that the inverted low-light images look like haze images. According to this observation, these methods have applied to deal with low-light images. However, these methods can obtain reasonable results, they has not provided a physical explanation for the basic model.

Retinex-based methods have been proposed for color images based on human visual system (HVS). According to the basic assumption of the Retinex theory [13], an observed image can be decomposed into two parts: the reflectance and illumination components. Early attempts in the field, such as Single-Scale Retinex (SSR) [6] and Multi-Scale Retinex (MSR) [7], treat the reflectance component as the enhancement result. However, these methods cause over-enhancement and generate unrealistic result. This problem is mainly caused by the logarithmic operation. To overcome this problem, Fu proposed proposed simultaneous reflectance and illumination estimation (SRIE) [8] and a weighted variation model (WVM) [9], and demonstrated that the linear domain model is better than the log-transformed domain in preserving naturalness. These methods have good performances in the enhancement, but they still have the problem that noise is quite observable in the results, especially when an observed image has much noise in dark regions. By considering the properties of 3D objects, Cai *et al.* [11] proposed a Joint intrinsic-extrinsic Prior (JieP) model for Retinex decomposition. However, the model is prone to over-smooth both the reflectance and illumination, since the model cannot sufficiently consider the constraint term about the reflectance. Moreover, Li presented a robust Retinex model (RRM) [12] by adding a noise term to the cost function to deal with low light image enhancement

under hidden noise. RRM suppresses noise amplification effectively, but it has difficulty balancing piecewise smoothed illumination and the structure of the reflectance.

Although many above methods adopt the L_1 norm to the reflectance, the tiny details of the estimated reflectance are susceptible to be damaged. Furthermore, by adopting the L_2 norm to the illumination, the estimated illumination over-smooths and loses the structure information.

In this paper, we propose a new joint optimization equation that considers the features of both reflectance and illumination. We adopt L_2-L_p norm regularization terms to estimate the reflectance as much as possible to preserving tiny details, and to estimate the illumination as much as possible to keep the structure information while avoiding texture-copy problem. Moreover, we introduce a new adaptive texture prior to handle much noise hidden in dark regions and to reveal details and textures of the estimated reflectance. Finally, in the experimental results including qualitative and quantitative evaluations, we show that the proposed method is more effective than the other several state-of-the-art methods.

Chapter 2

Related Work

2.1 Retinex Theory

The Retinex theory [13] is a color perception model based on human visual system. The model decomposes an observed image into the reflectance and illumination as follows:

$$S = R \circ I, \quad (2.1)$$

where S is an observed image, R and I represent the reflectance and the illumination, respectively. The operator \circ denotes the element-wise multiplication. As shown in Fig. 2.1, the reflectance represents the intrinsic characteristics of the object and contains rich textures detail. On the contrary, the illumination represents the extrinsic property and contains the structure information with texture-less.

The conventional Retinex-based enhancement methods such as [6], [7] are defined as

$$\log R = \log S - \log [G * S], \quad (2.2)$$

where $*$ represents the convolution operator, G is the Gaussian low-pass filter. This method assumes that illumination can be estimated by the Gaussian low-pass filtered version of an observed image. Moreover, the reflectance is computed by subtracting the estimated illumination from an observed image. However, this method generates the halo effect around the edges of object according to the size of the Gaussian low-pass filter. In addition, as shown in Fig. 2.2, this method cause over-enhancement and much noise in the estimated reflectance.

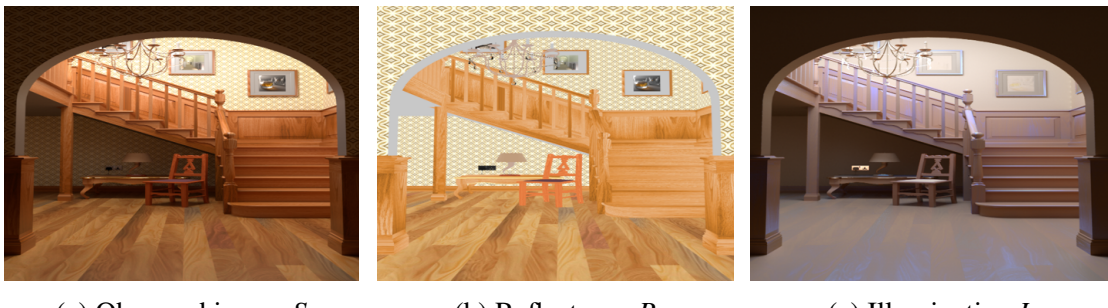


Figure 2.1: The images represent Retinex theory [16].



(a) Observed image S

(b) Reflectance R

Figure 2.2: The images represent the result of the conventional Retinex-based enhancement method [7].

2.2 Variational Retinex Model

Various researches have proposed energy minimization problems based on Retinex in order to efficiently estimate reflectance and illumination. These methods estimate reflectance and illumination by setting the constraint terms which consider the characteristics for their component. Thus, it is important for these methods to adopt the appropriate constraints for their component in order to deal with halo effect, over-enhancement, and noise amplification. These methods usually adopt the L_1 and L_2 norm regularization to the constraint terms. To give an example, Fu [8] proposed the minimizing optimization problem derived as

$$E(I, R) = \arg \min_{R, I} \|R \circ I - S\|_2^2 + \alpha \|\nabla I\|_2^2 + \beta \|\nabla R\|_1 + \gamma \|I - I_0\|_2^2 \\ s.t. \quad S \leqq I, \quad (2.3)$$

where α, β, γ are three positive parameters, and I_0 is the enhanced illumination using gamma correction. The first term $\|R \circ I - S\|_2^2$, which corresponds to L2 data fidelity, is to minimize the distance between the estimated $(R \circ I)$ and an observed image S . The second term $\|\nabla I\|_2^2$ enforces spatially smoothness on the illumination I . The third term $\|\nabla R\|_1$, which corresponds to TV reflectance sparsity, enforces piece-wise continuous on the reflectance R . The last term $\|I - I_0\|_2^2$, which penalizes the brightness of illumination component, is used to avoid a scaling problem.

This method demonstrated the linear domain model is better than the log-transformed domain model in preserving naturalness. As shown in Fig. 2.3, this method employs the third term which minimizes the difference between I and I_0 for the sake of suppression of over-enhancement in the estimated reflectance. Moreover, this method can suppress noise amplification due to the L_1 norm regularization on the reflectance in the estimated reflectance.

2.3 Local Variation Deviation

In this section, the review centers on the edge/structure preserving image smoothing and the joint intrinsic-extrinsic prior model (JieP), which proposed by Cai [11] and adopted

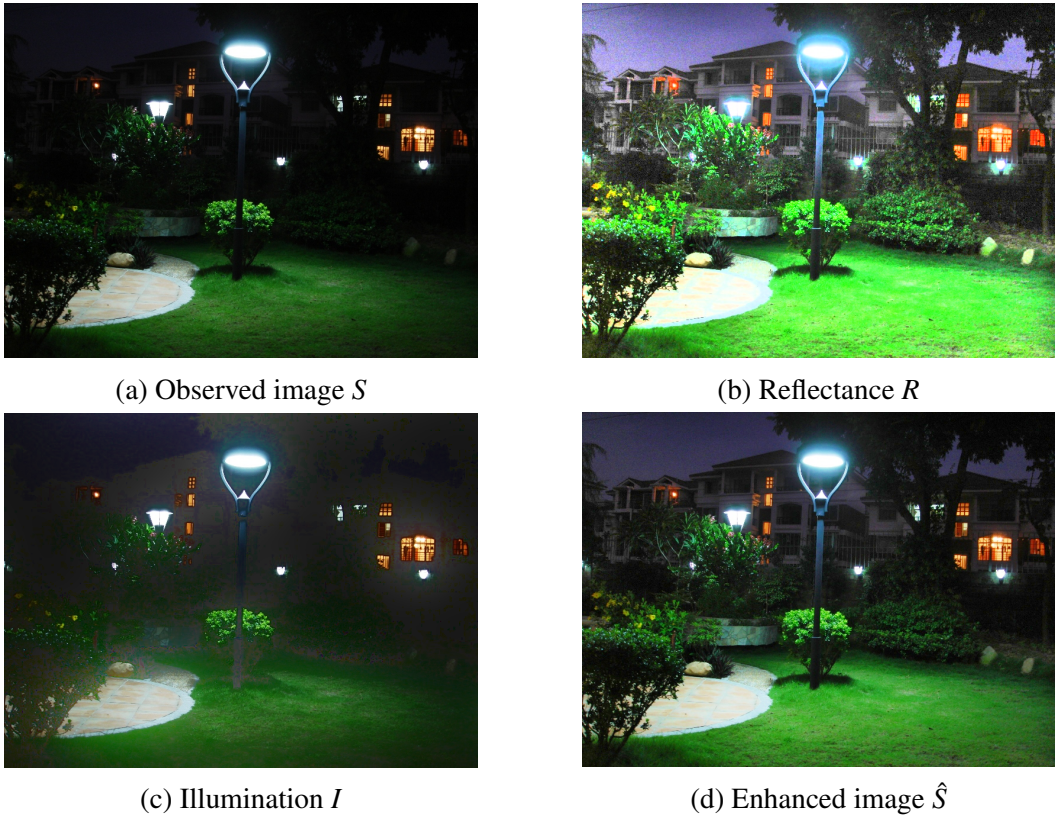


Figure 2.3: The images represent the result of SRIE [8].

the image smoothing function as the constraint term on the illumination in (2.3).

In statics, the standard deviation represents a measure to quantify the consistency of a set of data. The local variation deviation (LVD) is used to identify different type of the variation with its statistical property. By using the feature in the image analysis, the local variation deviation can surprisingly distinguish between texture and structure, since texture component has the feature of weak correlation and structure component has the feature of strong correlation.

The \mathcal{R}_d denotes the relative LVD extracted from I :

$$\mathcal{R}_d = \left| \frac{\nabla_d I}{\frac{1}{\Omega} \sum_{\Omega} \nabla_d I + \epsilon} \right|, \quad (2.4)$$

where ∇_d is the horizontal/vertical ($d \in h, v$) gradient operator, Ω is the local patch size ($r \times r$), and ϵ is a small number to avoid division by zero. The edge/structure preserving smoothing property of the LVD can be explained intuitively as following. (In the following, the variable of the mean local variation means $\bar{\nabla}I = \frac{1}{|\Omega|} \sum_{\Omega} \nabla I$):

- Case1: **Flat.** If the value of the patch I is almost constant, $\nabla I \approx 0$ and $\bar{\nabla}I \approx 0 \rightarrow \bar{\mathcal{R}} \approx 0$.
- Case2: **Texture.** If the value of the patch I changes frequently, ∇I varies more rapidly than $\bar{\nabla}I \rightarrow \bar{\mathcal{R}} \gg 1$.

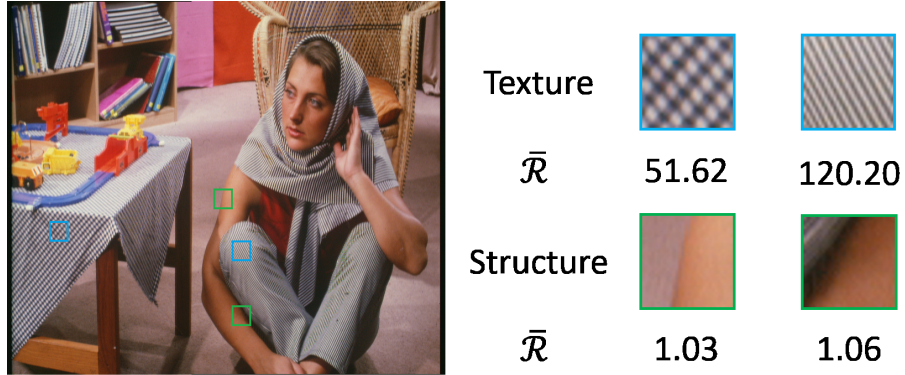


Figure 2.4: The images represent local variation deviation for different patches. \bar{R} is the average of variation deviation in the local patches. The local variation deviation surprisingly distinguish textures (blue regions) and structures (green regions).

- Case3: **Structure.** If the value of the patch I changes in accordance with structure, the deviation of ∇I fluctuates small $\rightarrow \bar{R} \approx 1$.

To quantitatively analyze the effectiveness of the distinction of the LVD measure, Fig.2.4 shows the average value of the LVD in the local patches. The blue regions represent textures and the green regions represent structures. As shown in Fig.2.4, there is a clear difference between texture and structure regions.

Thanks to the performance of the LVD, Cai replaced the constraint term on the illumination with the LVD on the illumination in the minimization optimization problem as following:

$$E(I, R) = \arg \min_{R, I} \|R \circ I - S\|_2^2 + \alpha \left\| \frac{\nabla I}{\frac{1}{\Omega} \sum_{\Omega} \nabla I + \epsilon} \right\|_1 + \beta \|\nabla R\|_1 + \gamma \|I - B\|_2^2, \quad (2.5)$$

where α, β, γ are three positive parameters and B ($B = \max_{\Omega}(\max_{c \in \{r, g, b\}} S_c)$) represents the bright channel prior (BCP) of an observed image S . As shown in Fig.2.5, the estimated illumination removes texture component while preserving the structure information. Thus, in the estimated reflectance, JieP significantly suppresses the awareness of halo effect along with edge regions. Moreover, more textures detail reveal in the estimated reflectance.

2.4 Consideration of Problems

These methods can enhance low-light images by solving each minimization optimization problem. However, these methods have some problems in the enhanced image or the estimated component. Therefore, in this section, the discussion centers on such problems with connected images.

- **SRIE.** This method is prone to over-smooth the illumination component without preserving the structure information because of the constraint term L_2 that the illumination should be spatially smooth. As a result, as shown in Fig. 2.6a, the estimated reflectance generates halo effect along with edge regions that have large intensity

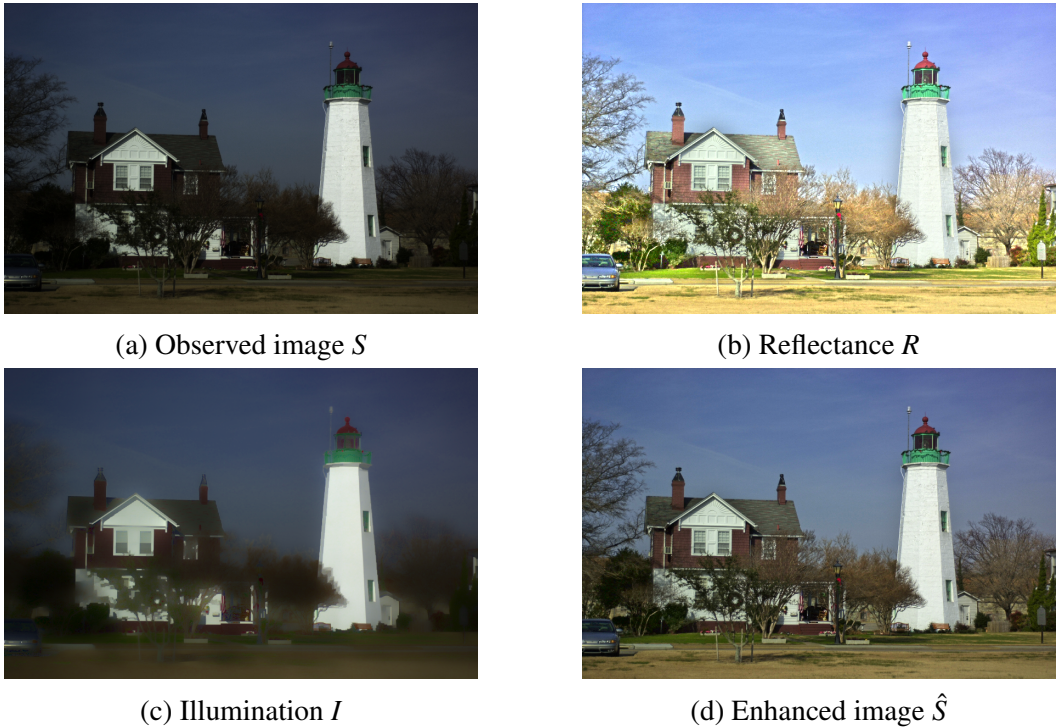


Figure 2.5: The images represent the result of JieP [11].

gradient. Moreover, as can be seen in Fig. 2.3b, in the estimated reflectance, much noise remain in dark regions and over-enhancement cause in bright regions because the constraint term on the reflectance is lack of the weight to distinguish between dark and bright regions.

- **JieP.** This method can significantly take consideration of the constraint term on the illumination, but is not sufficient for the reflectance. Therefore, as can be seen in Fig. 2.6b, the estimated reflectance have much noise in dark regions and over-enhance in bright regions. Moreover, the constraint term on the illumination adopts L1 norm regularization, so that it may damage structure information too much in the estimated illumination.



(a) Reflectance (SRIE)



(b) Reflectance (JieP)

Figure 2.6: The images represent each problem of these methods.

Chapter 3

Proposed Method

In this section, the discussion centers on the proposed method which improves the problems described in Sec.2.4. First, the $L_2 - L_p$ variational retinex model which further considers the feature of the reflectance and illumination is introduced in Sec. 3.1. Second, adaptive texture map which adaptively constraint noise amplification in dark regions and over-enhancement in bright regions is described in Sec. 3.2. Finally, the effectiveness of the proposed method is shown in comparison with the related work by using the output of some images in Sec. 3.4.

Fig. 3.1 shows the flowchart of the proposed method. To explain the flow of the proposed method briefly, the proposed method obtains a low-light image and the initialized illumination which is called the bright channel prior. Next, the proposed method converses a low-light image to HSV-Color scale and extract only value (V) channel. The proposed method iteratively solves the sub-problems related with the reflectance and illumination and gets their component which meet the constraints are appropriate for each component. Finally, the proposed method multiply the estimate reflectance and illumination, converses the obtained enhanced image to RGB-Color space.

3.1 L2-LP Variational Model

The conventional methods adopt the L_1 norm to the constraint term on the reflectance, but the fine detail of the estimated reflectance are susceptible to be damaged. Furthermore, by adopting the L_2 norm to the constraint term on the illumination, the estimated illumination over-smooths and loss the structure information. Therefore, the proposed method adopts $L_2 - L_p$ norm regularization to each constraint term in order to estimate the reflectance as much as possible to preserve tiny details and estimate the illumination as much as possible to keep the structure information while removing texture component. The new joint optimization equation is given as:

$$E(I, R) = \arg \min_{R, I} \|R \circ I - S\|_2^2 + \alpha \left\| \frac{\nabla I}{\frac{1}{\Omega} \Sigma_\Omega \nabla I + \epsilon} \right\|_p^p + \beta \|W \circ \nabla R\|_2^2 + \gamma \|I - B\|_2^2, \quad (3.1)$$

where $\|\cdot\|_p$ denotes the L_p norm regularization term ($0 < p \leq 2$), and W is adaptive texture map related to the reflectance R . As described in [15], a block coordinate descent [17] is used in order to find an optimal solution to the non-convex objective function (3.1). Since

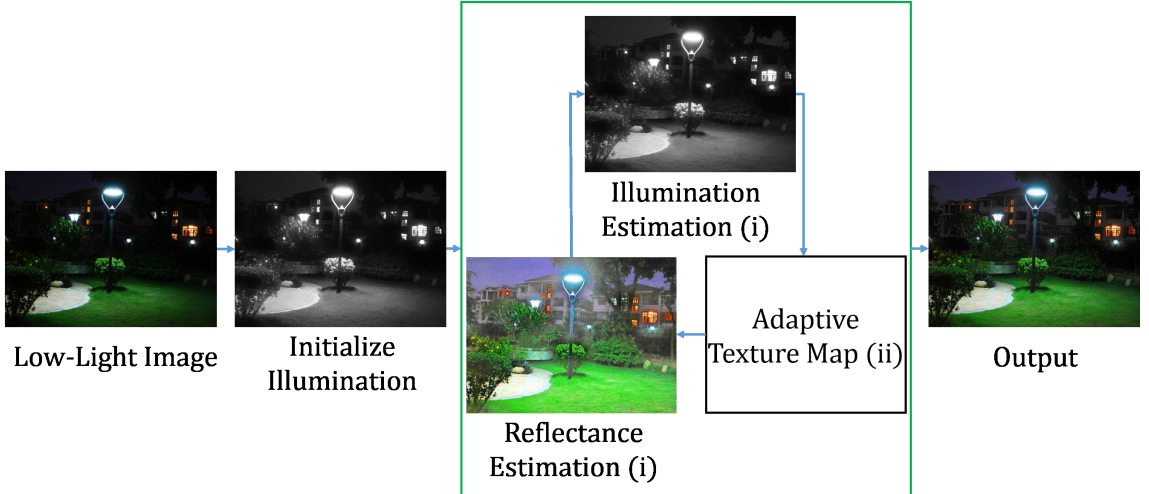


Figure 3.1: The image represents the flowchart of the proposed method. (i)The proposed method changes the constraint terms further considered the characteristics for each component. (ii)The proposed method generates adaptive texture map to constrain noise amplification and over-enhancement in the estimated reflectance.

the L_p regularization term causes non-smooth optimization, the proposed method adopts an iteratively re-weighted least square (IRLS) method [18] and rewrite the second term in (3.1) as:

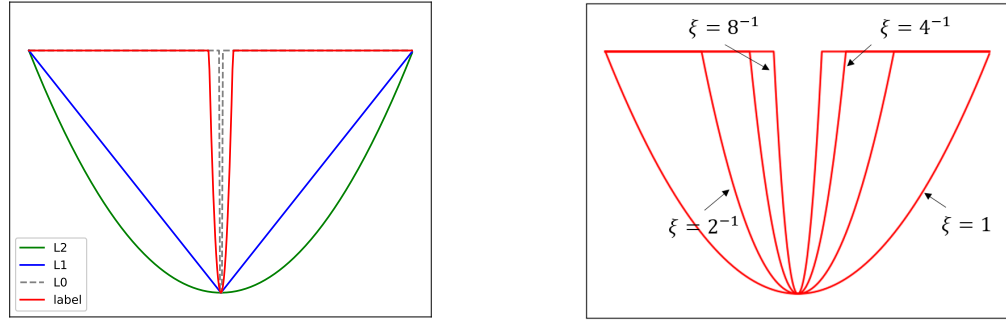
$$\left\| \frac{\nabla I}{\frac{1}{\Omega} \Sigma_{\Omega} \nabla I + \epsilon} \right\|^p = \|U \circ \nabla I\|^2, \quad (3.2)$$

$$U = \begin{cases} \frac{1}{\xi^{2-p}}, & \left| \frac{\nabla I}{\frac{1}{|\Omega|} \Sigma_{\Omega} \nabla I} \right| < \xi \\ \frac{|\Sigma_{\Omega} \nabla I|^{2-p}}{|\nabla I|^{2-p}} \frac{1}{|\Sigma_{\Omega} \nabla I|^2}, & \text{otherwise} \end{cases} \quad (3.3)$$

$$= \begin{cases} \frac{1}{\xi^{2-p}}, & \left| \frac{\nabla I}{\frac{1}{|\Omega|} \Sigma_{\Omega} \nabla I} \right| < \xi \\ \frac{1}{|\Sigma_{\Omega} \nabla I|^p |\nabla I|^{2-p}}, & \text{otherwise} \end{cases} \quad (3.4)$$

where the variable u is only approximate variable. This is because the Eq. 3.2 uses a L_2 norm format $\Phi(\frac{\nabla I}{\frac{1}{\Omega} \Sigma_{\Omega} \nabla I + \epsilon}; \xi)$ based on [19] to approximate the L_0 norm function. As can be seen in Fig. 3.2a, the red curve can approximate the most sparse L_0 function. Therefore, the proposed method can remove fine textures and preserve meaningful salient structures in the estimated illumination. As shown in Fig. 3.2b, with the decease of the value ξ , the L_p norm function is getting close to the L_0 function. Therefore, large- ξ are more convex-like and easy to optimize, in contrast, small- ξ are more steep and difficult to optimize.

Fig. 3.3 shows the effect of changing the value of p in the range $(0 < p \leq 2)$ in the estimated illumination. As the value of p decreases, the estimated illumination leaves smooth and texture-less. Concomitantly, the estimated reflectance contains more rich textures and details. In particular, when $p = 0$, some salient structure information in the estimated illumination may be lost too much, because the L_0 norm has strong sparsity.



(a) Plots of different penalty functions (b) Plots of L_p norm for different values p

Figure 3.2: The images represent various plots about the L_p norm.

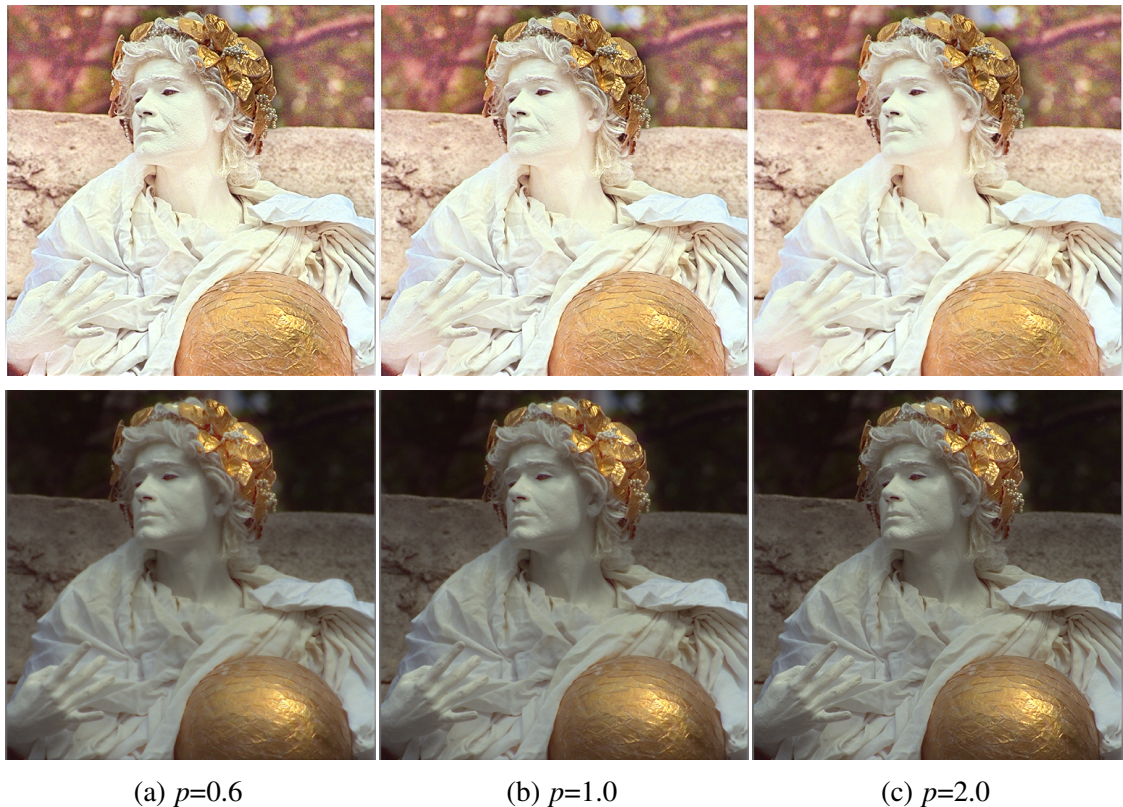


Figure 3.3: Comparison of decomposition results for different values of norm p . ((a)-(c) top: reflectance, bottom: illumination)

3.2 Adaptive Texture Map

The discussion centers on the effect of the adaptive texture map using as the weight of the constraint term on the reflectance. Discussed in Sec. 2.1, reflectance component contains rich details. However, when the reflectance is enhanced, noise hidden in dark regions amplifies and over-enhancement cause in bright regions. Therefore, the weight which controls these problems is necessary for the constraint term on the reflectance. In addition, the preferable reflectance's gradients should be smooth in homogeneous regions while undamaged at edges and texture regions. Thus, when estimating the reflectance, the weight which can recognize more texture regions is required. Fig. 3.4 shows the summary of the above discussion. Then, the adaptive texture map W is set so that the third term performs strong noise reduction in dark and homogeneous regions, while it performs weak noise reduction in bright and textures regions. The formulation of W is given as:

$$W_d = W_B \circ A_d, \quad (3.5)$$

where d represents horizontal (h) and vertical (v) directions, and W_B represents the initial estimated weight map by inverting the normalized bright channel, and A_d represents the texture map that effectively distinguish between homogeneous and textures regions.

In the same way as in [21], given an observed low-light image, the adaptive texture map can selectively assign different values according to BCP since the estimated bright channel contains large values in bright regions and vice versa. Thus, W_B is given as:

$$W_B = 1.0 - \max_{c \in \{r,g,b\}} S^c. \quad (3.6)$$

Fig. 3.5 shows the image of W_B . Since smaller weight values are assigned in bright regions, W_B performs the weaker noise reduction. In contrast, stronger noise reduction is performed in dark regions.

Moreover, texture map A_d is set as the inverse of the a_r -th power of the absolute value of a mean local variation (MLV) [11], so that it can significantly distinguish between homogeneous regions and texture regions:

$$A_d = \frac{1}{\left| \frac{1}{|\Omega|} \sum_{\Omega} \nabla_d R \right|^{a_r} + \epsilon}, \quad (3.7)$$

where $a_r (< 1)$ is an exponential parameter to adjust the texture awareness for the reflectance. As shown in Fig. 3.6b, when $a_r = 1.0$, the texture map A_d extracts salient edges but little texture component. In contrast, when $a_r = 0.5$, it extract both salient edges and rich texture component. Therefore, using the texture map, W performs weaker noise reduction in both edges and texture regions, on the other hand, stronger noise reduction in homogeneous regions.

Comparing Fig. 3.7a and 3.7b, we see that the estimated reflectance with W can suppress over-enhancement in bright regions and noise amplification in dark regions. Moreover, the estimated reflectance with W can reveal details and textures in spite of noise reduction.

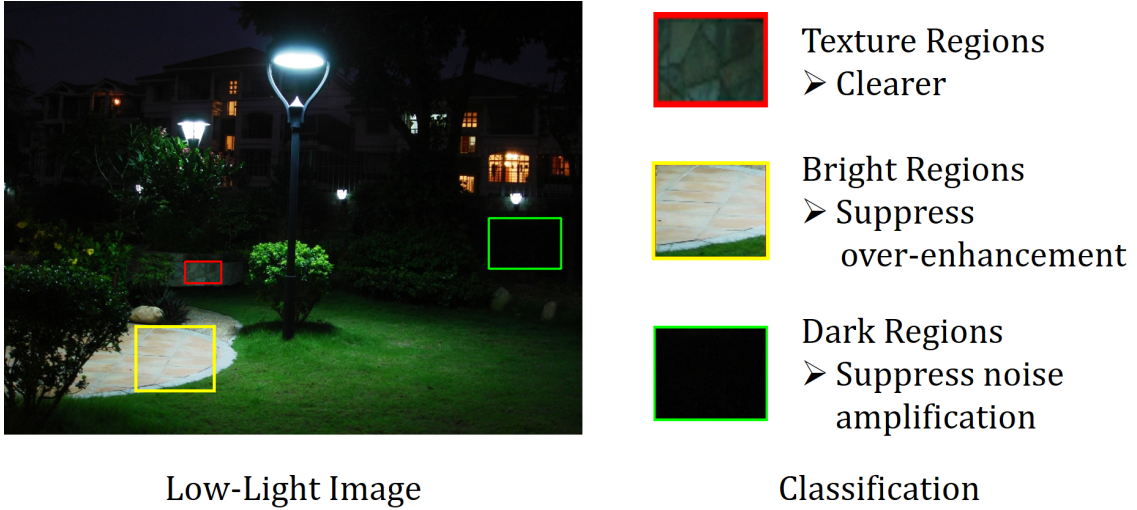


Figure 3.4: The image represents the classification of regions where the adaptive texture map has an impact on.



Figure 3.5: The image represents W_B . W_B contains smaller values in bright regions, in contrast, larger values in dark regions.

3.3 Solution

The minimization optimization problem (3.1) can be solved by iteratively updating each component. In particular, for the k -th iteration of sub-problems.

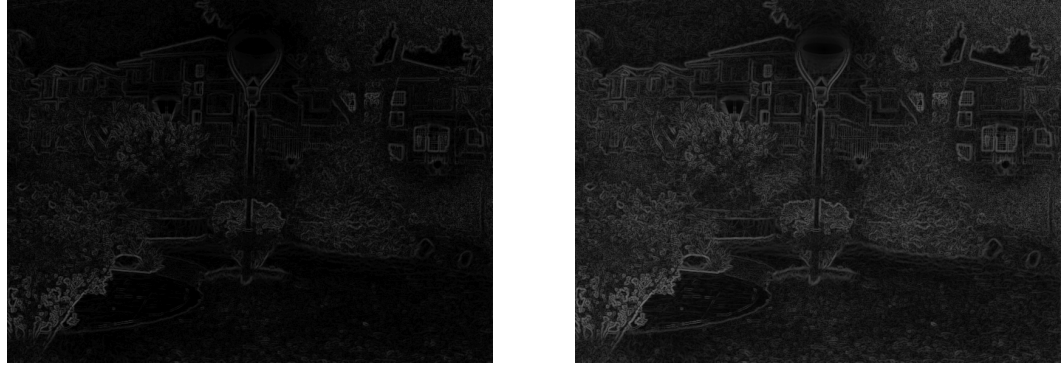
- 1). **I sub-problem:** Collecting the terms related to I leads to the following equation (3.1):

$$I_k = \arg \min_I \|R_{k-1} \circ I - S\|_2^2 + \alpha \|U \circ \nabla I\|_2^2 + \lambda \|I - B\|_2^2. \quad (3.8)$$

We reduce the equation (3.8) to a classic least square problem:

$$i_k = \arg \min_i \|r_{k-1} \hat{i} - s\|_2^2 + \alpha \|\hat{D} i\|_2^2 + \lambda \|i - b\|_2^2, \quad (3.9)$$

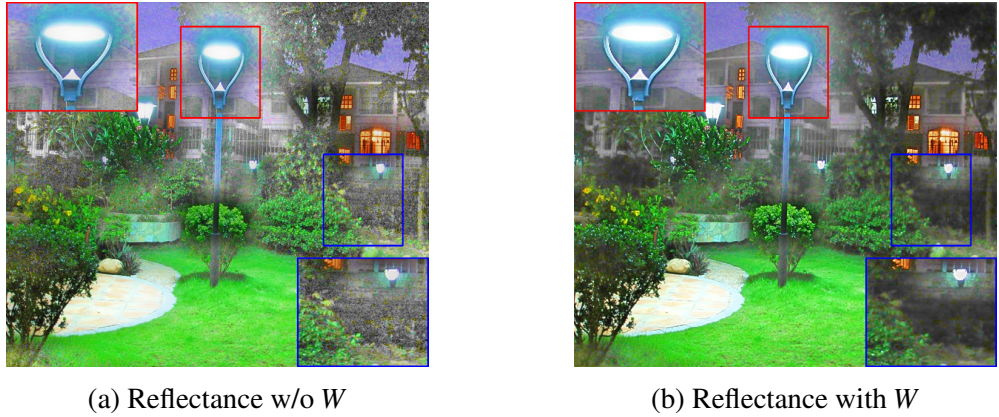
where i is the vectorized format of I and \hat{i} represents a diagonal matrix with i as its entries, and D contains D_h and D_v , which are the Toeplitz matrices from the



(a) MLV ($a_r = 1.0$)

(b) MLV ($a_r = 0.5$)

Figure 3.6: Comparison of MLV results for different values of a_r . As the value of a_r decreases, MLV can obtain more rich gradient information.



(a) Reflectance w/o W

(b) Reflectance with W

Figure 3.7: Comparison of reflectance results. (a) the estimated reflectance without W ; (b) the estimated reflectance with W .

discrete gradient operators with forward difference. The same notation is used for other matrices (r , s , b corresponds to R , S , and B , respectively). By differentiating equation (3.9) with respect to i , and setting the derivative to 0, we have the following solution:

$$i_{k+1} = (\hat{r}_{k-1}\hat{r}_{k-1}^T + \alpha D^T \hat{u}D + \lambda I)^{-1}(\hat{r}_{k-1}^T s + \lambda \hat{b}). \quad (3.10)$$

Then, we reformulate the obtained i_k into matrix format I_k .

- 2). **R sub-problem:** After acquiring I_k from the above solution, the joint optimization (3.1) related to R becomes similar to that of I :

$$R_k = \arg \min_R \|R \circ I_k - S\|_2^2 + \beta \|W \circ \nabla R\|_2^2. \quad (3.11)$$

In the same way as in the former derivation, we provide the solution of R as follows:

$$r_k = (\hat{i}_k \hat{i}_k^T + \beta D^T \hat{w}D)^{-1}(\hat{i}_k^T s). \quad (3.12)$$

Similarly, we reformulate the obtained r_k into matrix format R_k .

The values of I and R are updated until $\|I_k - I_{k-1}\|/\|I_{k-1}\| \leq \varepsilon$ and $\|R_k - R_{k-1}\|/\|R_{k-1}\| \leq \varepsilon$ are simultaneously satisfied. After the estimation of the reflectance and illumination, a Gamma correction operation is adopted to adjust the illumination. Therefore, the final enhanced image is given as $S_{enhanced} = R \circ I^{\frac{1}{\gamma'}}$, where the empirical parameter γ' is set as 2.2. To preserve color information, the Gamma correction is performed in the HSV domain.

3.4 Effectiveness of the proposed method

Chapter 4

Experiment

Acknowledgement

I would like to give heartfelt thanks to Prof. Youji Iiguni who provided fruitful suggestions and helpful comments and help in interpreting the significance of this study. I also appreciate to Associate Prof. Ryota Shimokura who provided helpful comments and suggestions in practical aspect. Finally, I would like to thank all the Bachelor, Master, Doctor students in Iiguni laboratory.

Reference

- [1] E. D. Pisano *et al*, “Contrast limited adaptive histogram equalization image processing to improve the detection of simulated speculations in dense mammograms,” *J. Digit. Image*, vol. 11, no. 4, pp. 193-200, 1998.
- [2] H. Cheng and X. Shi, “A simple and effective histogram equalization approach to image enhancement,” *Digital Signal Processing*, vol. 14, no. 2, pp. 158-170, 2004.
- [3] S.-C. Huang, F.-C. Cheng, and Y.-S. Chiu, “Efficient contrast enhancement using adaptive gama correction with weighting distribution,” *IEEE Trans. Image Process.*, vol. 20, no. 5, pp. 1262-1272, 2011.
- [4] L. Li, R. Wang, W. Wamg, and W. Gao, “A low-light image enhancement method for both denoising and contrast enlarging,” in *Proc. IEEE Int. Conf. Image Process.*, pp. 3730-3734, 2015.
- [5] X.Zhang, P.Shen, L. Luo, L. Zhang, and J. Song, “Enhancement and noise reduction of very low light level images,” in *Proc. 21st Int. Conf. Pattern Recognit. (ICPR)*, pp. 2034-2037, 2012.
- [6] D. J. Jobson, Z.-U. Rahman, and G. A. Woodell, “Properties and performance of a center/surround retinex,” *IEEE Trans. Image Process.*, vol. 6, no. 3, pp. 451-462, 1997.
- [7] D. J. Jobson, Z.-U. Rahman, and G. A. Woodell, “A multiscale retinex for bridging the gap between color images and the human observation of scenes,” *IEEE Trans. Image Process.*, vol. 6, no. 7, pp. 965-976, 1997.
- [8] X. Fu, Y. Liao, D. Zeng, Y. Huang, X. Zhang, and X. Ding, “A probabilistic method for image enhancement with simultaneous illumination and reflectance estimation,” *IEEE Trans. Image Process.*, vol. 24, no. 12, pp. 4965-4977, 2015.
- [9] X. Fu, D. Zeng, Y. Huang, X. Zhang and X. Ding, “A weighted variational model for simultaneous reflectance and illumination estimation, ” *IEEE Conf. Computer Vis. Pattern Recognit.*, pp. 2782-2790, 2016.
- [10] X. Guo, Y. Li, and H. Ling, “LIME: Low-light image enhancement via illumination map estimation,” *IEEE Trans. Image Process.*, vol. 26, no. 2, pp. 982-993, 2017.
- [11] B. Cai, X. Xu, K. Guo, K. Jia, B. Hu, and D. Tao, “A joint intrinsic-extrinsic prior model for retinex,” In *Proc., IEEE Conf. Computer Vis., Pattern Recognit.*, pp. 4000-4009, 2017.

- [12] M. Li, J. Liu, W. Yang, X. Sun, and Z. Guo, “Structure-revealing low-light image enhancement via robust Retinex model,” IEEE Trans. Image Process., vol. 27, no. 6, pp. 2828-2841, 2018.
- [13] E. H. Land and J. J. McCann, “Lightness and retinex theory,” J. Opt. Soc. Amer., vol. 61, no. 1, pp. 1-11, 1971.
- [14] K. He, J. Sun, and X. Tand, “Guided image filtering,” Proc. European Conf. on Computer Vis., pp. 1-14, 2010.
- [15] C. Fu, L. Duan, and C. Xiao, “A hybrid L2-Lp variational model for single low-light image enhancement with bright channel prior,” IEEE Int. Conf. on Image Process. (ICIP), 2019.
- [16] N. Bonneel, B. Kovacs, S. Paris, and K. Bala, “Intrinsic decompositions for image editing,” Computer Graphics Forum, vol.36, no. 2, 2017.
- [17] P. Tseng, “Convergence of a block coordinate descent method for nondifferentiable minimization,” Journal of Optimization Theory and Applications, vol. 109, no. 3, pp. 475-494, 2001.
- [18] E. J. Candes, M. B. Wakin, and S. P. Boyd, “Enhancing sparsity by reweighted l_1 minimization,” Journal of Fourier Analysis and Applications, vol. 14, no. 5-6, pp. 877-905, 2008.
- [19] L. Xu, S.Zheng, and J. Jia, “Unnatural 10 sparse representation for natural image deblurring,” IEEE Conf. Computer Vis. Pattern Recognit., pp. 1107-1114, 2013.
- [20] X. Fu, D. Zheng, Y. Huang, X. Ding, and X-P. Zhang, “A variational framework for single low light image enhancement using bright channel prior,” in Proc. IEEE Global Conf. on Signal and Inform. Process., pp. 1085-1088, 2013.
- [21] S. Park, S. Yu, B. Moon, S. Ko, and J. Paik, “Low-light image enhancement using variational optimization-based retinex model,” IEEE Trans. on Cons. Elec., vol. 63, no. 2, pp. 178-184, 2017.
- [22] S. Wang, J. Zheng, H.-M. Hu, and B. Li, “Naturalness preserved enhancement algorithm for non-uniform illumination images,” IEEE Trans. Image Process., vol. 22, no. 9, pp. 3538-3578, 2013.
- [23] K. Gu, G. Zhai, W. Lin, X. Yang, and W. Zhang, “No reference image sharpness assessment in autoregressive parameter space,” IEEE Trans. on Image Process., vol. 24, no. 10, pp. 3218-3231, 2015.